

Coulomb excitation of hydrogen atoms by vortex ion beams

Anna V. Maiorova

*Helmholtz Institute Jena, D-07743 Jena, Germany and
GSI Helmholtzzentrum für Schwerionenforschung GmbH, D-64291 Darmstadt, Germany*

Dmitry Karlovets

-

Stephan Fritzsche

*Helmholtz Institute Jena, D-07743 Jena, Germany
GSI Helmholtzzentrum für Schwerionenforschung GmbH, D-64291 Darmstadt, Germany and
Theoretisch-Physikalisches Institut, Friedrich-Schiller-Universität Jena, D-07743 Jena, Germany*

Andrey Surzhykov

*Physikalisch-Technische Bundesanstalt, D-38116 Braunschweig, Germany
Institut für Mathematische Physik, Technische Universität Braunschweig, D-38106 Braunschweig, Germany and
Laboratory for Emerging Nanometrology Braunschweig, D-38106 Braunschweig, Germany*

Thomas Stöhlker

*Helmholtz Institute Jena, D-07743 Jena, Germany
GSI Helmholtzzentrum für Schwerionenforschung GmbH, D-64291 Darmstadt, Germany and
Institut für Optik und Quantenelektronik, Friedrich-Schiller-Universität Jena, D-07743 Jena, Germany*

(Dated: March 27, 2024)

Coulomb excitation of hydrogen atoms by vortex protons is theoretically investigated within the framework of the non-relativistic first-Born approximation and the density matrix approach. Special attention is paid to the magnetic sublevel population of excited atoms and, consequently, to the angular distribution of the fluorescence radiation. We argue that both these properties are sensitive to the projection of the orbital angular momentum (OAM), carried by the projectile ions. In order to illustrate the OAM-effect, detailed calculations have been performed for the $1s \rightarrow 2p$ excitation and the subsequent $2p \rightarrow 1s$ radiative decay of a hydrogen target, interacting with incident Laguerre-Gaussian vortex protons. The calculation results suggest that Coulomb excitation can be employed for the diagnostics of vortex ion beam at accelerator and storage ring facilities.

I. INTRODUCTION

Investigations of vortex, or twisted, states of light and matter have a rich history of more than thirty years. These states, which possess a helical phase front and carry a non-zero projection l_{OAM} of the orbital angular momentum (OAM) onto their propagation direction, were first predicted and experimentally realized for the *photon* beams in the early nineties of the last century [1, 2]. Since then, vortex light has found its applications in many areas of modern physics, ranging from super-resolution microscopy and magnetometry to classical and quantum information processing, operation of atomic clock transitions and optical tweezing [3–8]. Following the success of twisted photon research, Bliokh and co-workers in 2007 [9] predicted and described the properties of free *electron* states with non-zero OAM projection and phase vortices. Having been produced just a few years later [10–13], the OAM electrons rapidly demonstrated their unique potential for transmission electron microscopy (TEM), probing magnetic properties of materials and for studying light-matter coupling [11, 14–16]. The next particles produced in the vortex state were *neutrons* [17, 18]. This opens up fundamentally new pos-

sibilities for quantum tomography of neutron states, as well as for studies in hadronic and low-energy nuclear physics. Finally, the successful experimental realization of vortex *atoms* and even *molecules* was reported in 2021 [19], providing a novel tool for investigations of fundamental interactions, chirality and parity violation.

A natural extension of the above-mentioned research of vortex states of light and matter is positively-charged *ions* in accelerator and storage ring facilities. The OAM projection of vortex ions will deliver an additional and very intriguing degree of freedom for collision studies in atomic and nuclear physics. However, the realization of these collision experiments requires the development of techniques for production and diagnostics of vortex ions. For the former task, two approaches were proposed recently that are based on the use of (i) forked diffraction gratings, similar to those in Ref. [19], or (ii) magnetized stripping foils [20]. Both methods can generate low-intensity Laguerre-Gaussian (LG) ion beams with the OAM projection l_{OAM} and the transverse coherence length up to the μm range. To verify the non-zero l_{OAM} of the produced vortex beams, their intensity profile can be measured, as was demonstrated for neutral atoms in Ref. [19]. An alternative and very promising approach for

the OAM–diagnostics is based on the analysis of fundamental atomic processes, induced in collisions with vortex ions. In the present work, we discuss the feasibility of this approach for the example of Coulomb excitation and subsequent radiative decay of target atoms. A number of studies of such a two step “excitation and decay” process have been performed in the past for conventional (plane–wave) projectiles [21–24]. These studies have demonstrated that angular distribution and polarization of the decay radiation uniquely reflect the magnetic sublevel population of excited target atoms and, consequently, details of collisions. Here, we will extend theoretical studies of Coulomb excitation towards Laguerre–Gaussian projectiles to demonstrate the sensitivity (of the properties) of this process to the OAM projection.

In our study, we will focus on the $1s \rightarrow 2p$ excitation of hydrogen atoms, bombarded by Laguerre–Gaussian protons, $H(1s) + H_{LG}^+ \rightarrow H(2p) + H^+$. This process can be naturally described in the framework of non–relativistic first–Born approximation, whose basic ideas and formulas are presented in Section II A. By making use of Born transition amplitudes and the density matrix approach we derive in Section II B the total excitation probability and the alignment parameter, that describe the magnetic sublevel population of the $2p$ hydrogenic state. In Section II C both of these parameters are used to predict the angular distribution of the $2p \rightarrow 1s$ radiation for both the case of a single H atom and for a *macroscopic* hydrogen target. For the latter case, which is of particular interest for future experiments, it is shown that the angular distribution of fluorescence photons is indeed sensitive to the OAM projection of incident protons. Detailed calculations supporting this conclusion, and hence the practical applicability of Coulomb excitation for the diagnostics of vortex ion beams, are presented in Section III. Finally, the paper is concluded by a short summary in Section IV.

II. THEORY

A. Excitation amplitude

In the present work we consider the excitation of a hydrogen–like ion from an initial $|n_i l_i m_i\rangle$ to a final state $|n_f l_f m_f\rangle$ due to the Coulomb interaction with a projectile ion. We assume that the ion is prepared in a Laguerre–Gaussian (LG) state [20, 25], which is an *exact solution* of the free time-dependent Schrödinger equation and whose properties will be discussed below. For theoretical analysis of the excitation process, it is convenient to choose the quantization axis (z -axis) of the entire system parallel to the mean velocity $\mathbf{v}_p = (0, 0, v_p)$ of the ionic wave packet, see Fig. 1. Together with the target atom, that we place at the origin, the direction of the mean velocity of the twisted beam defines the reaction plane (xz -plane), wherein the center of the LG wave packet is shifted from the atom by an impact parameter $\mathbf{b} = (b, 0, 0)$. The position of the atomic electron relative

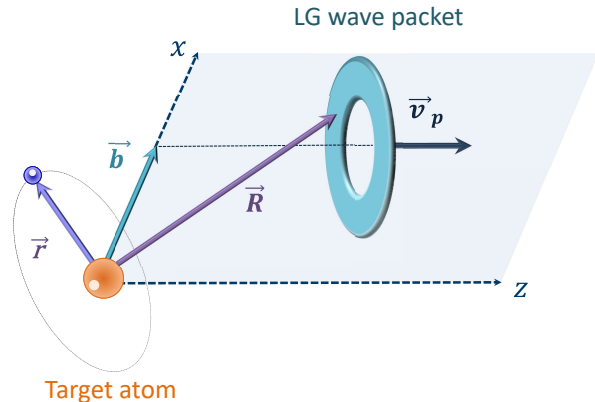


FIG. 1. Geometry of Coulomb excitation of the hydrogen-like atom by the vortex ion beam representing the Laguerre–Gaussian wave packet.

to the target nucleus is determined by the vector \mathbf{r} , while the vector $\mathbf{R} = (R_x, R_y, R_z) \equiv (\mathbf{R}_\perp, R_z)$ characterizes the charge density of the wave packet as “seen” from the target, see Fig. 1.

After discussing the geometry and basic notations, we are ready to proceed with the theoretical analysis of the Coulomb excitation process. Within the non–relativistic framework, the Hamiltonian of a hydrogen atom, interacting with a charged projectile, can be written in the form:

$$\hat{H} = -\frac{\hbar^2}{2m} \nabla^2 - \frac{e^2}{r} + V(\mathbf{r}, t) \equiv \hat{H}_0 + \hat{V}(\mathbf{r}, t). \quad (1)$$

Here, the first two terms represent the usual (unperturbed) Hamiltonian of the hydrogen atom, while the perturbation is given by the interaction

$$\hat{V}(\mathbf{r}, t) = -Z_p e^2 \int \frac{\rho(\mathbf{R}, t) d\mathbf{R}}{|\mathbf{r} - \mathbf{R}|}, \quad (2)$$

between the bound electron and the ionic wave packet with charge Z_p and time–dependent (normalized) charge density $\rho(\mathbf{R}, t)$. Thus, our approach resembles the well established semi–classical theory of atomic collisions, in which a projectile moves along a classical trajectory.

For the case of a non–relativistic Laguerre–Gaussian wave packet with the orbital angular momentum l_{OAM} and a principal quantum number $n = 0$, the density $\rho(\mathbf{R}, t)$ can be written in the following form [20, 25, 26]:

$$\begin{aligned} \rho(\mathbf{R}, t) &\equiv |\Psi^{LG}(\mathbf{R} - \mathbf{b}, t)|^2 \\ &= \frac{1}{\sqrt{\pi^3}} \frac{1}{|l_{OAM}|!} \frac{1}{\sigma_z(t) \sigma_\perp^2(t)} \left(\frac{(\mathbf{R}_\perp - \mathbf{b})^2}{\sigma_\perp^2(t)} \right)^{|l_{OAM}|} \\ &\times \exp \left[-\frac{(\mathbf{R}_\perp - \mathbf{b})^2}{\sigma_\perp^2(t)} - \frac{(R_z - v_p t)^2}{\sigma_z^2(t)} \right], \quad (3) \end{aligned}$$

where the proton wave function $\Psi^{LG}(\mathbf{R}, t)$ obeys the free time-dependent Schrödinger equation exactly (see the Appendix). Here $\sigma_{\perp}(t)$ and $\sigma_z(t)$ are widths of the wave packet in transverse and longitudinal directions, respectively. Assuming no dispersion of the projectile wave packet during the collision ($\tau \sim 1 ns$), we will assume below that both the transverse and longitudinal widths of the packet do not depend on time: $\sigma_{\perp}(t) \equiv \sigma_{\perp}$ and $\sigma_z(t) \equiv \sigma_z$. This assumption fits well with the estimate of the spreading time of an ion:

$$t_d = \frac{\sigma_{\perp}^2(t = t_0)}{c \lambda_c}, \quad (4)$$

where λ_c is the proton Compton wavelength, see Appendix and Ref. [20] for further details. Since the typical transverse coherence length of the produced Laguerre–Gaussian ion wave packet is about $\sigma_{\perp}(t = t_0) \sim 1 \mu m$, the typical spreading time $t_d \sim 10^{-6}$ s is few orders of magnitude larger than the reaction duration.

Having briefly discussed the Hamiltonian (1) of the system, we consider the time-dependent Schrödinger equation:

$$i\hbar \frac{\partial \Psi(\mathbf{r}, t)}{\partial t} = \hat{H} \Psi(\mathbf{r}, t), \quad (5)$$

whose solution $\Psi(\mathbf{r}, t)$ can be constructed in terms of eigenfunctions $\varphi_k(\mathbf{r})$ and eigenvalues ε_k of the unperturbed Hamiltonian \hat{H}_0 :

$$\Psi(\mathbf{r}, t) = \sum_k a_k(t) \varphi_k(\mathbf{r}) \exp(-i\varepsilon_k t). \quad (6)$$

By employing the wave function $\Psi(\mathbf{r}, t)$ one can obtain the probability

$$\mathcal{P}_f = |\langle \varphi_f | \Psi(\mathbf{r}, t) \rangle|^2 = |a_f(t \rightarrow +\infty)|^2 \quad (7)$$

to find the target atom into some specific final state $|\varphi_f\rangle$ after the collision, i.e. at $t \rightarrow +\infty$.

As seen from Eq. (7), the analysis of the excitation of the target hydrogen atom by the vortex projectile is traced back to the evaluation of the amplitude $a_f(t \rightarrow +\infty)$. In general, this is a very challenging task because of the summation over the entire atomic spectrum in the wave function $\Psi(\mathbf{r}, t)$. Indeed, \sum_k in Eq. (6) indicates the summation over bound $|k\rangle = |nlm\rangle$ and integration over continuum hydrogenic states. The evaluation of the transition amplitude can be greatly simplified, however, within the framework of the first Born approximation:

$$\begin{aligned} a_f(t \rightarrow +\infty) &\equiv a_{fi} = \\ &= -i \int_{-\infty}^{\infty} \exp(-i\omega_{if} t) \langle \varphi_f | \hat{V}(\mathbf{r}, t) | \varphi_i \rangle dt. \end{aligned} \quad (8)$$

Here we assume a well defined initial state of the atom, $\varphi_i = \Psi(\mathbf{r}, t \rightarrow -\infty)$, and introduce the notation $\omega_{if} = \varepsilon_i - \varepsilon_f$ for the transition energy.

With the help of the first-Born amplitude $a_f(t \rightarrow +\infty)$ we can investigate the excitation $|i\rangle = |n_i l_i m_i\rangle \rightarrow |f\rangle = |n_f l_f m_f\rangle$ of the hydrogen atom due to the Coulomb interaction with the Laguerre–Gaussian ion wave packet. Indeed, by inserting the interaction operator (2) into Eq. (8) and by employing the non-relativistic hydrogenic solutions $\varphi_{nlm}(\mathbf{r}) = R_{nl}(r) Y_{lm}(\theta, \phi)$ we found, after some algebra:

$$\begin{aligned} a_{fi}(\mathbf{b}) &= \frac{i Z_p e^2}{\pi v_p \sigma_{\perp}^2 |l_{OAM}|} \exp\left(-\left(\frac{\omega_{if} \sigma_z}{2v_p}\right)^2\right) \\ &\times \sum_{LM} \frac{4\pi}{2L+1} \langle l_f m_f | Y_{LM}^* | l_i m_i \rangle I_{LM}(\mathbf{b}), \end{aligned} \quad (9)$$

where we introduced the notation:

$$\begin{aligned} I_{LM}(\mathbf{b}) &= \int d\Omega_R \left[Y_{LM}(\hat{\mathbf{R}}) \int dR dr R^2 r^2 \right. \\ &\times \frac{r_{<}^L}{r_{>}^{L+1}} R_{n_f l_f}(r) R_{n_i l_i}(r) \left(\frac{(\mathbf{R}_{\perp} - \mathbf{b})^2}{\sigma_{\perp}^2} \right)^{|l_{OAM}|} \\ &\times \exp\left(-\frac{i\omega_{if} R_z}{v_p}\right) \exp\left(-\frac{(\mathbf{R}_{\perp} - \mathbf{b})^2}{\sigma_{\perp}^2}\right) \left. \right], \end{aligned} \quad (10)$$

with $r_{>} = \max(r, R)$ and $r_{<} = \min(r, R)$. The evaluation of the four-dimensional integral (10) is in general a rather complicated task which can be simplified, however, by using *analytical* solutions $R_{nl}(r)$ of the Schrödinger equation for a point-like target nucleus.

B. Cross section and alignment parameter

In previous subsection we have derived the expression for the amplitude Eq. (9) of the atomic transition, induced by the interaction with a projectile Laguerre–Gaussian wave packet. This amplitude, which depends both on the impact parameter \mathbf{b} and on the size, velocity and OAM of the wave packet, can be used to derive all observables of the Coulomb excitation process. In the present work, we focus on the $|1s\rangle \rightarrow |2p\rangle$ excitation whose total probability is given by:

$$\mathcal{P}_{\text{tot}}(\mathbf{b}) = \sum_{m_f=0, \pm 1} |a_{2p m_f}(\mathbf{b})|^2, \quad (11)$$

where the summation runs over all magnetic substates $|2p m_f\rangle$ of the final excited state.

Apart from the total excitation probability $\mathcal{P}_{\text{tot}}(\mathbf{b})$, we can use the amplitude (9) to investigate the magnetic sublevel population of the ion. Most naturally it is described within the framework of the density matrix theory in terms of the so-called alignment parameters A_{kq} [21, 27–29]. For an atom in the p -state, i.e. with $l_f = 1$, there are in general five alignment parameters A_{2q} with

$-2 \leq q \leq 2$ in addition to the trivial one $A_{00} \equiv 1$. While the parameter

$$A_{20}(\mathbf{b}) = \sqrt{2} \frac{|a_{2p m_f = \pm 1}(\mathbf{b})|^2 - |a_{2p m_f = 0}(\mathbf{b})|^2}{|a_{2p m_f = 0}(\mathbf{b})|^2 + 2|a_{2p m_f = \pm 1}(\mathbf{b})|^2} \quad (12)$$

describes the relative population of the magnetic substates $|2p m_f\rangle$ and is expressed in terms of the transition amplitudes squared, the parameters A_{2q} with $q \neq 0$ characterise the coherence between these substates [21, 30].

Similar to the total excitation probability $\mathcal{P}_{\text{tot}}(b)$, the alignment of the $2p$ state also depends on the position of the target atom b and on the parameters of the incident wave packet. Hence, its measurements can provide more insight into the interaction of atomic targets with vortex ion beams.

C. Angular distribution of fluorescence emission

After excitation, the excited atomic state will decay into the ground one by the emission of a photon. The angular distribution (as well as the polarization) of this subsequent decay is directly related to the relative population of magnetic sublevels, as described by the set of alignment parameters [31, 32]. For the $|2p\rangle \rightarrow |1s\rangle$ decay, for example, the angular distribution of emitted radiation can be generally written as:

$$W_b(\theta, \phi) = \mathcal{P}_{\text{tot}}(b) \left(1 + \sqrt{\frac{4\pi}{5}} \sum_q \frac{A_{2q}(\mathbf{b})}{\sqrt{2}} Y_{2q}(\theta, \phi) \right), \quad (13)$$

where the polar θ and azimuthal ϕ angles determine the direction of photon emission with respect to the quantization (z -) axis and reaction (xz -) plane, respectively.

The angular distribution (13) is derived for a rather academic case of a single target atom, localized at the distance b from the center of the incident Laguerre–Gaussian wave packet, see Fig. 1. In realistic experiments, which can be performed at linear accelerator or ion storage ring, the vortex ions will interact not with a single atom but with a *macroscopic* atomic target. To estimate the angular distribution of the $2p \rightarrow 1s$ radiation, emitted from such a target, we have to average the “individual” contributions (13) over the impact parameter b :

$$\begin{aligned} W_{\text{lab}}(\theta) &= \int W_b(\theta, \phi) d^2\mathbf{b} \\ &= \tilde{\sigma}_{\text{tot}} \left(1 + \frac{\tilde{A}_{20}}{\sqrt{2}} P_2(\cos \theta) \right). \end{aligned} \quad (14)$$

Here we have assumed a homogeneous target whose atoms contribute incoherently to the decay emission. Moreover, the *effective* excitation cross section $\tilde{\sigma}_{\text{tot}}$ and the alignment \tilde{A}_{20} are introduced in the second line of

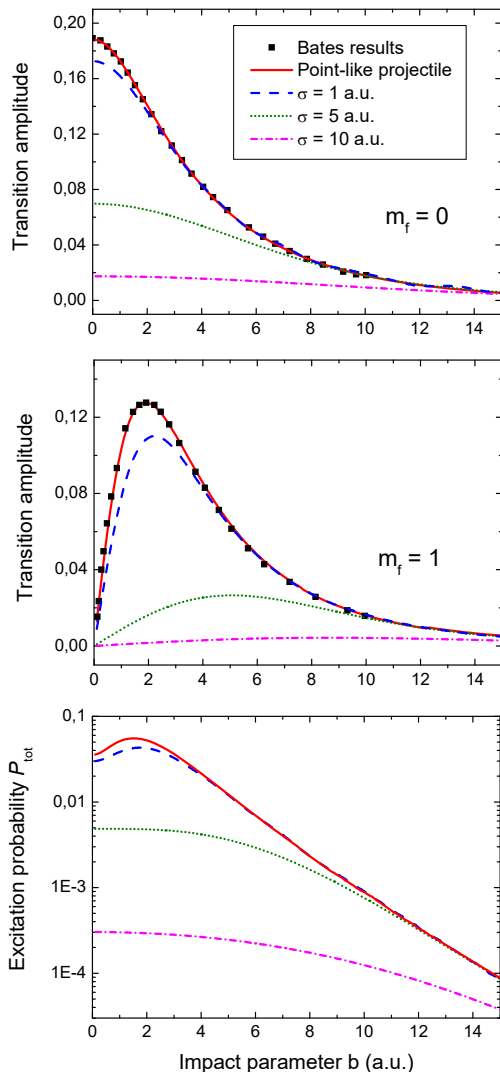


FIG. 2. The absolute values of the transition amplitude $a_{2p m_f = 0}(\mathbf{b})$ (upper panel) and $a_{2p m_f = \pm 1}(\mathbf{b})$ (middle panel), as well as the total excitation probability $\mathcal{P}_{\text{tot}}(\mathbf{b})$ (bottom panel) as functions of the impact parameter b . The calculations were carried out for a point H^+ projectile (red solid line), as well as for the Gaussian wave packets with the transverse widths $\sigma_{\perp} = 1$ a.u. (blue dashed line), $\sigma_{\perp} = 5$ a.u. (green dotted line) and $\sigma_{\perp} = 10$ a.u. (pink dash-dotted line). The point-like projectile results are compared with the previous predictions (black squares) by Bates [33]. Note that the bottom panel uses a logarithmic scale to better illustrate the dependence of the excitation probability on the packet width.

Eq. (14). Both $\tilde{\sigma}_{\text{tot}}$ and \tilde{A}_{20} are obtained from Eqs. (11) and (12), respectively, where the b -averaged squared amplitudes $|\tilde{a}_{2p m_f}|^2 = \int |a_{2p m_f}(\mathbf{b})|^2 b db$ are employed in place of $|a_{2p m_f}(\mathbf{b})|^2$.

As seen from Eq. (14), the angular distribution $W_{\text{lab}}(\theta)$ of the decay radiation from a macroscopic homogeneous target is defined by the single (effective) alignment parameter \tilde{A}_{20} and does not depend on the azimuthal angle ϕ . This is an obvious implication of the azimuthal

symmetry of the system “LG ion beam *plus* macroscopic target”, and can be trivially obtained by integrating Eq. (13) over ϕ_b when using the standard transformation of the alignment parameters $A_{2q}(\mathbf{b}) = e^{iq\phi_b} A_{2q}(b)$, with $q = 0, \pm 1, \pm 2$, see Ref. [34] for further details.

III. RESULTS AND DISCUSSION

In the present work, we focus on the $1s \rightarrow 2p$ excitation and subsequent radiative decay of the hydrogen target in collisions with the Laguerre–Gaussian proton beam, i.e. for $Z_p = 1$. Our special interest to the $H(1s) + H^+$ collisions stems from the fact that they have been extensively studied in the past for the conventional *plane-wave* projectiles. The well-established plane-wave results will serve as a benchmark for our calculations and will help us to better emphasize the effect of ion’s OAM in Coulomb excitation of the target atoms.

Before proceeding to analyze the OAM-dependence of the Coulomb excitation, let us briefly discuss the effect of the another key parameter of our theory – the width of the incident wave packet. In Fig. 2, we display the absolute values of the transition amplitudes a_{2p0} and $a_{2p\pm 1}$ as functions of the impact parameter b . Here, the black solid squares display the predictions by Bates [33], obtained within the framework of the first-Born approximation and when describing the projectile as a point-like charge, moving along the straight trajectory $\mathbf{R}(t) = \mathbf{b} + \mathbf{v}_p t$. We reproduce well these previous results by employing the delta-function limit ($\sigma_z \rightarrow 0$, $\sigma_\perp \rightarrow 0$, $l_{OAM} = 0$) of the wave packet charge density (3), see red solid line in the figure. Moreover, calculations were performed for incident wave packets with $l_{OAM} = 0$, but with non-vanishing width $\sigma_\perp = 1$ a.u. (blue dashed line), $\sigma_\perp = 5$ a.u. (green dotted line) and $\sigma_\perp = 10$ a.u. (pink dash-dotted line). As seen from the figure, both transition amplitudes are very sensitive to the transverse spread of the wave packet. For example, the maximum of $|a_{2p\pm 1}|$ decreases and its position shifts towards larger impact parameters as the width σ_\perp becomes larger. Also absolute values of $|a_{2p0}|$ quickly diminish with increasing the width; the effect that is most pronounced for small impact parameters b .

Having briefly recalled the sensitivity of the $1s \rightarrow 2p$ Coulomb excitation to the transverse size of the incident wave packet, we are ready to investigate the effect of the OAM projection. We start with the case of a single hydrogen atom, being initially in the ground $1s$ state and displaced by the distance b from the axis of the Laguerre Gaussian beam (3). For this case, we display in Fig. 3 the total excitation probability $\mathcal{P}_{\text{tot}}(b)$ (top panel) and the alignment parameter $A_{20}(b)$ of the $2p$ state (bottom panel). The results are presented for the incident wave packet with the mean energy $T_p = 5$ MeV/u, the transverse width $\sigma_\perp = 100$ a.u., and with three different OAM projections: $l_{OAM} = 0$ (red solid line), $l_{OAM} = 1$ (blue dashed line), and $l_{OAM} = 2$ (green dotted line).

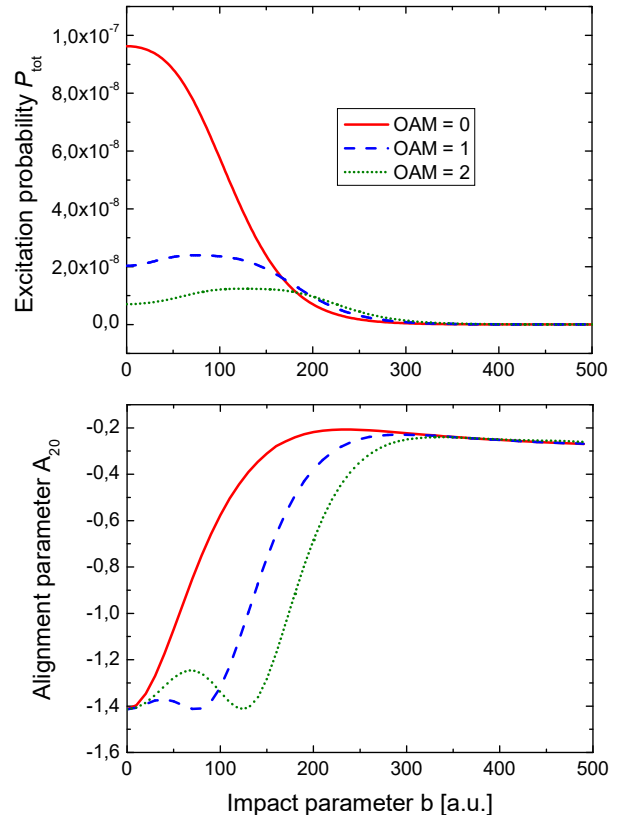


FIG. 3. Total excitation probability (top) and alignment parameter (bottom) for Coulomb excitation of the hydrogen atom by the vortex proton wave packet with the energy $T_p = 5$ MeV/u, the width $\sigma_\perp = \sigma_z = 100$ a.u. and various OAM projections: $l_{OAM} = 0, 1, 2$, as functions of the impact parameter b .

As follows from the figure, both the excitation probability and the alignment parameter strongly depend on the OAM projection of the vortex ion beam. In particular, one can observe a substantial decrease of $\mathcal{P}_{\text{tot}}(b)$ for higher OAM projections. The total excitation probability drops almost tenfold for an atom, located on the wave packet axis, $b = 0$, and interacting with the Laguerre–Gaussian beam ($l_{OAM} = 2$) instead of the Gaussian one ($l_{OAM} = 0$). The significant reduction of $\mathcal{P}_{\text{tot}}(b = 0)$ can be explained by qualitatively distinct charge densities (3) of the wave packets with $l_{OAM} = 0$ and $l_{OAM} \neq 0$: while the $\rho(l_{OAM} = 0)$ is maximal at $b = 0$, the $\rho(l_{OAM} \neq 0)$ exhibits the annual ring structure with the low-density spot around the beam center.

Besides the total excitation probability, the alignment parameter $A_{20}(b)$ also exhibits a remarkable sensitivity to the OAM projection of projectile ions. As seen from the bottom panel of Fig. 3, Coulomb excitation by the vortex projectile ions ($l_{OAM} \neq 0$) can lead to a much stronger alignment of the $2p$ state when comparing to the $l_{OAM} = 0$ case. Indeed, $|A_{20}(b, l_{OAM} = 0)| < |A_{20}(b, l_{OAM} \neq 0)|$.

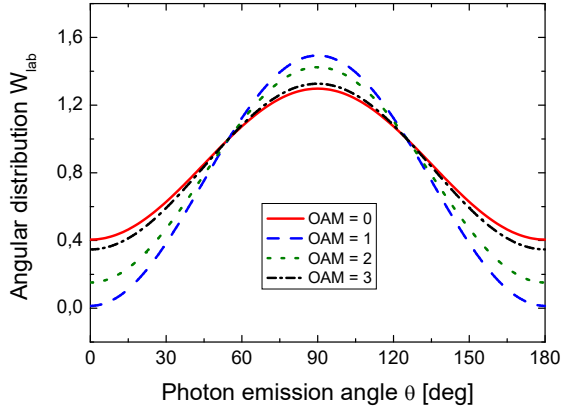


FIG. 4. Angular distribution of the $|2p\rangle \rightarrow |1s\rangle$ radiative decay following Coulomb excitation of hydrogen atoms by Laguerre–Gaussian proton beam. Since we are primarily interested in the *shape* of the angular distribution, all $W_{lab}(\theta)$ are normalized here as $\int W_{lab}(\theta) d\Omega = 1$. The characteristics of the ion beam are the same as for Fig. 3.

$0\rangle$ for $0 < b \lesssim 200$ a.u., i.e. in the range of impact parameters for which the probability $\mathcal{P}_{tot}(b)$ is large, thus indicating that collisions with Laguerre Gaussian wave packets favor the population of the $|2p m_f = 0\rangle$ substate. As it will be shown below, this behaviour of the alignment of the excited $2p$ state allows one to diagnose the OAM of ion beams for a realistic scenario of collisions with a macroscopic atomic target.

The angle–resolved measurements of photoemission from target atoms, excited in collisions with projectile ions, are one of the best–established methods to study the magnetic sublevel population of (excited) atom [21, 27, 28]. While in the past, this method has been widely applied for conventional plane–wave projectiles, here we propose to extend it for the diagnostics of Laguerre–Gaussian beams. In order to advocate the feasibility of such (future) experiments, we display in Fig. 4 the angular distribution of $2p \rightarrow 1s$ radiation, emitted from the *macroscopic* hydrogen target bombarded by protons with $l_{OAM} = 0$ (red solid line), $l_{OAM} = 1$ (blue dashed line), $l_{OAM} = 2$ (green dotted line) and $l_{OAM} = 3$ (black dash-dotted line). The angular distribution was calculated based on Eq. (14), for the transverse beam’s spread $\sigma_{\perp} = 100$ a.u. and mean energy $T_p = 5$ MeV/u. As seen from the figure, the anisotropy of the $2p \rightarrow 1s$ emission is rather sensitive to the l_{OAM} of projectile ions. This sensitivity reflects the OAM–dependence of the effective alignment parameter \tilde{A}_{20} that enters Eq. (14) and that is displayed in Fig. 5. Indeed, the most pronounced anisotropy of fluorescence emission can be observed for Coulomb excitation of the hydrogen target by protons, carrying the OAM projection $l_{OAM} = 4$, for which $\tilde{A}_{20} = -0.9240$. In contrast, the excitation of the macroscopic hydrogen target by the Gaussian beam with

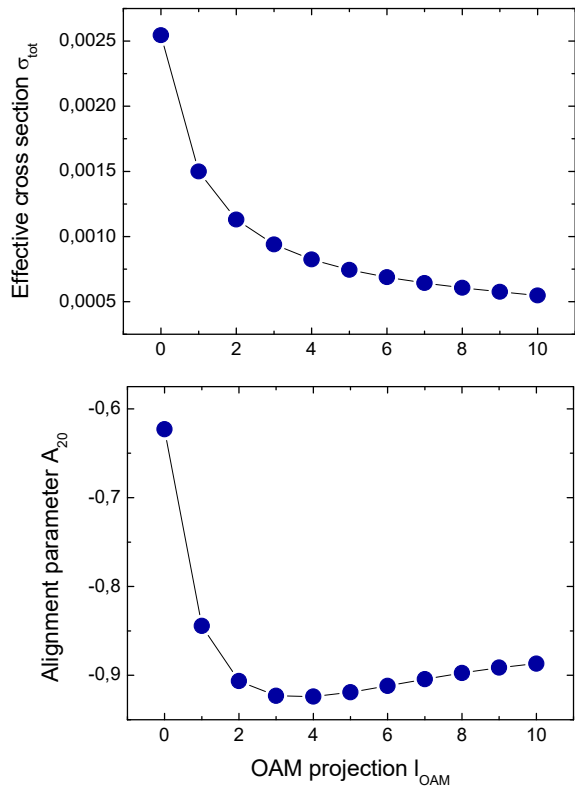


FIG. 5. Effective excitation cross section $\tilde{\sigma}_{tot}$ (top panel) and alignment parameter \tilde{A}_{20} (bottom panel) for the macroscopic hydrogen target, bombarded by the LG proton wave packet with the energy $T_p = 5$ MeV/u and transverse width $\sigma_{\perp} = 100$ a.u. Results are presented for various OAM projections.

$l_{OAM} = 0$ leads to the effective alignment $\tilde{A}_{20} = -0.6229$ and, hence, to a weaker anisotropy of the radiation pattern. This variation of the $2p \rightarrow 1s$ angular distribution for different OAM projections can easily be observed with the modern detectors and can open a route for the diagnostics of vortex ion beams.

IV. SUMMARY

In this work we have theoretically studied the Coulomb excitation of one–electron atoms by Laguerre–Gaussian ionic wave packets. Special attention was paid to the question of how the population of the magnetic sublevels of the excited atom is affected by the OAM projection of the projectile ions. In order to explore this OAM–dependence, we have applied the non–relativistic first–Born approximation and the density matrix theory. The general expressions were derived for the total excitation probability and the alignment parameter of the excited

atom. Based on the theory obtained, detailed calculations have been carried out for the $\text{H}(1s) + \text{H}_{LG}^+ \rightarrow \text{H}(2p) + \text{H}_{LG}^+$ excitation of hydrogen atoms by vortex proton beam. In these calculations, we have addressed not only a rather academic case of the excitation of a single well-localized atom, but also the much more promising—from the experimental viewpoint—scenario of collision of the ion beam with the macroscopic hydrogen target. For the latter case, particular emphasis was placed on the angular distribution of the subsequent $2p \rightarrow 1s$ radiative emission from the whole target, which is defined by the magnetic sublevel population of excited atoms and which can be easily measured in modern experiments. We have clearly shown that the anisotropy of the $2p \rightarrow 1s$ radiation and, hence, the alignment of the $2p$ state are very sensitive to the OAM projection of the Laguerre–Gaussian beam. This sensitivity opens us a very promis-

ing avenue for the diagnostics of vortex ion beams in accelerator and storage ring experiments

ACKNOWLEDGEMENTS

A.S. acknowledges support by the Deutsche Forschungsgemeinschaft (DFG, German Research Foundation) under Germany's Excellence Strategy – EXC-2123 QuantumFrontiers – 390837967.

APPENDIX: WAVE FUNCTION OF THE TWISTED PROTON

Apart from the well-known plane wave, the Laguerre–Gaussian wave packet:

$$\begin{aligned} \Psi^{LG}(\mathbf{R}, t) = & \sqrt{\frac{n!}{(n + |\ell_{OAM}|)!}} \frac{1}{\pi^{3/4}} \left(\frac{R_{\perp}}{\sigma_{\perp}(t)} \right)^{|\ell_{OAM}|} \frac{1}{\sigma_{\perp}(t) \sqrt{\sigma_z(t)}} L_n^{|\ell_{OAM}|} \left(\frac{R_{\perp}^2}{\sigma_{\perp}^2(t)} \right) \\ & \times \exp \left\{ -\frac{i}{\hbar} t \frac{\langle p \rangle^2}{2m_p} + \frac{i}{\hbar} \langle p \rangle R_z + \frac{i}{\hbar} \ell_{OAM} \phi_r - i(2n + |\ell_{OAM}| + 1) \arctan(t/t_{d,\perp}) - \frac{i}{2} \arctan(t/t_{d,z}) - \right. \\ & \left. - \frac{R_{\perp}^2}{2\sigma_{\perp}^2(t)} (1 - it/t_{d,\perp}) - \frac{(R_z - v_p t)^2}{2\sigma_z^2(t)} (1 - it/t_{d,z}) \right\}, \end{aligned} \quad (15)$$

with the standard normalization

$$\int d^3R |\Psi^{LG}(\mathbf{R}, t)|^2 = 1, \quad (16)$$

is also an exact solution of the free-particle Schrödinger equation. Here, $\mathbf{R} = \{R_{\perp} \cos \phi_r, R_{\perp} \sin \phi_r, R_z\}$, m_p is the proton mass, $\langle p \rangle = v_p m_p$ is a mean momentum, $n = 0, 1, 2, \dots$ is a principal quantum number and $l_{OAM} = 0, \pm 1, \pm 2, \dots$ is a projection of the orbital angular momentum onto the propagation axis.

The set of solutions (15) for $n = 0, 1, 2, \dots$ and $l_{OAM} = 0, 1, 2, \dots$ is *complete and orthogonal*. It describes, moreover, free rectilinear motion on average,

$$\langle R_z \rangle(t) = v_p t, \quad (17)$$

and spreading of the wave packet with time both in the transverse and longitudinal directions. For example, for the transverse direction one can find:

$$\begin{aligned} \sigma_{\perp}^2(t) &= \frac{\hbar^2}{(\sigma_{\perp}^p)^2} \left(1 + \frac{t^2}{t_{d,\perp}^2} \right) = \sigma_{\perp}^2(t_0) + \left(\frac{\sigma_{\perp}^p}{m_p} \right)^2 t^2, \\ \sigma_{\perp}(t_0) &= \frac{\hbar}{\sigma_{\perp}^p}, \end{aligned} \quad (18)$$

where

$$t_{d,\perp} = \frac{m_p \hbar}{(\sigma_{\perp}^p)^2} = \frac{\sigma_{\perp}^2(t_0)}{c \lambda_c} \quad (19)$$

is the time after which $\sigma_{\perp}(t_d) = \sqrt{2} \sigma_{\perp}(t_0)$, $\lambda_c = \hbar/m_p c$ is the Compton wavelength of the proton, and σ_{\perp}^p is the width of the wave packet in the momentum space. Similar expressions can be obtained for the longitudinal direction:

$$\begin{aligned} \sigma_z^2(t) &= \frac{\hbar^2}{(\sigma_z^p)^2} \left(1 + \frac{t^2}{t_{d,z}^2} \right) = \sigma_z^2(t_0) + \left(\frac{\sigma_z^p}{m_p} \right)^2 t^2, \\ \sigma_z(t_0) &= \frac{\hbar}{\sigma_z^p}, \quad t_{d,z} = \frac{m_p \hbar}{(\sigma_z^p)^2} = \frac{\sigma_z^2(t_0)}{c \lambda_c}. \end{aligned} \quad (20)$$

One can note that for both cases $t_{d,\perp}$ and $t_{d,z}$ are inversely proportional to $c \lambda_c = \hbar/m_p \approx 4 \times 10^{-7} \text{ m}^2/\text{s}$, which implies characteristic dispersion time of about $t_d \sim 10^{-6} \text{ s}$ for μm -size proton wave packets.

At large distances from the source compared to the Rayleigh length, the root-mean-square radius of the wave packet, which can be written in terms of the transverse spreading of the wave packet as $\langle R_{\perp}^2 \rangle(t) = \sigma_{\perp}^2(t) (2n + |l_{OAM}| + 1)$, spreads as [20]:

$$\sqrt{\langle R_{\perp}^2 \rangle(t)} \equiv \langle R_{\perp} \rangle = \lambda \frac{\langle R_z \rangle}{\langle R_{\perp} \rangle_0} (2n + |l_{OAM}| + 1), \quad (21)$$

with $\lambda = \hbar/\langle p \rangle$ is the de Broglie wavelength and $\langle R_{\perp} \rangle_0 \equiv \sqrt{\langle R_{\perp}^2 \rangle(t = t_0)}$. For the Gaussian mode with $n = 0$ and $l_{OAM} = 0$, this is simply the far-field *van Cittert–Zernike theorem*.

-
- [1] L. Allen, M. W. Beijersbergen, R. J. C. Spreeuw, and J. P. Woerdman, Orbital angular momentum of light and the transformation of laguerre-gaussian laser modes, *Phys. Rev. A* **45**, 8185 (1992).
- [2] H. He, M. E. J. Friese, N. R. Heckenberg, and H. Rubinsztein-Dunlop, Direct observation of transfer of angular momentum to absorptive particles from a laser beam with a phase singularity, *Phys. Rev. Lett.* **75**, 826 (1995).
- [3] H. He, M.E.J. Friese, N.R. Heckenberg, and H. Rubinsztein-Dunlop, Direct observation of transfer of angular momentum to absorptive particles from a laser beam with a phase singularity, *Phys. Rev. Lett.* **75**, 826 (1995).
- [4] G. C. G. Berkhout, M. W. Beijersbergen, Using a multi-point interferometer to measure the orbital angular momentum of light in astronomy, *Journal of Optics A: Pure and Applied Optics* **11**, 094021 (2009).
- [5] J.T. Barreiro, T.C. Wei, P.G. Kwiat, Beating the channel capacity limit for linear photonic superdense coding, *Nature Physics* **4**, 282 (2008).
- [6] M.J. Padgett, Orbital angular momentum 25 years on [Invited], *Opt.Express* **25**, 11265 (2017).
- [7] Y. Shen, Xu. Wang, Zh. Xie, Ch. Min, Xi Fu 1, Q. Liu, M. Gong and Xi. Yuan, Optical vortices 30 years on: OAM manipulation from topological charge to multiple singularities, *Light: Science & Applications* **8**, 90 (2019).
- [8] M. Babiker, D. L. Andrews, and V. E. Lembessis, Atoms in complex twisted light, *Journal of Optics* **21**, 013001 (2018).
- [9] K.Y. Bliokh, Y. P. Bliokh, S. Savel'ev, and F. Nori, Semiclassical dynamics of electron wave packet states with phase vortices, *Phys. Rev. Lett.* **99**, 190404 (2007).
- [10] M. Uchida and A. Tonomura, Generation of electron beams carrying orbital angular momentum, *Nature* **464**, 737 (2010).
- [11] J. Verbeeck, H. Tian, P. Schattschneider, Production and application of electron vortex beams, *Nature* **467**, 301 (2010).
- [12] B. J. McMorran, A. Agrawal, I. M. Anderson, A. A. Herzog, H. J. Lezec, J. J. McClelland, and J. Unguris, Electron vortex beams with high quanta of orbital angular momentum, *Science* **331**, 192 (2011).
- [13] E. Mafakheri, A. H. Tavabi, P.-H. Lu, R. Balboni, F. Venturi, C. Menozzi, G. C. Gazzadi, S. Frabboni, A. Sit, R. E. Dunin-Borkowski, E. Karimi, V. Grillo, Realization of electron vortices with large orbital angular momentum using miniature holograms fabricated by electron beam lithography, *Appl. Phys. Lett.* **110**, 093113 (2017).
- [14] S. Lloyd, M. Babiker, J. Yuan, Quantized orbital angular momentum transfer and magnetic dichroism in the interaction of electron vortices with matter, *Phys. Rev. Lett.* **108**, 074802 (2012).
- [15] J. Verbeeck, H. Tian, G. Van Tendeloo, How to manipulate nanoparticles with an electron beam?, *Advanced Materials* **25**, 1114 (2013).
- [16] J. Harris, V. Grillo, E. Mafakheri, G. C. Gazzadi, S. Frabboni, R. W. Boyd and E. Karimi, Structured quantum waves, *Nature* **11**, 629 (2015).
- [17] Ch.W. Clark, R. Barankov, M.G. Huber, M. Arif, D.G. Cory and D.A. Pushin, Controlling neutron orbital angular momentum, *Nature* **525**, 504 (2015).
- [18] H. Larocque, I. Kaminer, V. Grillo, R. W. Boyd, E. Karimi, Twisting neutrons may reveal their internal structure, *Nature Physics* **14**, 1 (2018).
- [19] A. Luski, Y. Segev, R. David, O. Bitton, H. Nadler, A. R. Barnea, A. Gorlach, O. Cheshnovsky, I. Kaminer, E. Nareviciu, Vortex beams of atoms and molecules, *Science* **373**, 1105 (2021).
- [20] D. Karlovets, Vortex particles in axially symmetric fields and applications of the quantum busch theorem, *New Journal of Physics* **23**, 033048 (2021).
- [21] K. Blum, *Density matrix theory and applications; 3rd ed.*, Springer Series on Atomic Optical and Plasma Physics (Springer, Berlin, 2012).
- [22] C. D. Lin, R. Shingal, A. Jain, and W. Fritsch, Orientation and alignment of collisionally excited atomic states, *Phys. Rev. A* **39**, 4455 (1989).
- [23] N. Andersen, D. Doweck, A. Dubois, J. P. Hansen, and S. E. Nielsen, Outer-shell excitation and capture processes: alignment and orientation effects, *Physica Scripta* **42**, 266 (1990).
- [24] J. Eichler, *Lectures on Ion-Atom Collisions*, North-Holland Personal Library (Elsevier Science, Amsterdam, 2005).
- [25] D. Karlovets, Relativistic vortex electrons: Paraxial versus nonparaxial regimes, *Phys. Rev. A* **98**, 012137 (2018).
- [26] B. Liu and I. P. Ivanov, Threshold effects in high-energy vortex state collisions, *Phys. Rev. A* **107**, 063110 (2023).
- [27] E. G. Berezhko and N. M. Kabachnik, Theoretical study of inner-shell alignment of atoms in electron impact ionisation: angular distribution and polarisation of x-rays and auger electrons, *Journal of Physics B: Atomic, Molecular and Optical Physics* **10**, 2467 (1977).
- [28] V. V. Balashov, A. N. Grum-Grzhimailo, and N. M. Kabachnik, *Polarization and correlation phenomena in atomic collisions* (Kluwer Academic/Plenum, New York, 2000).
- [29] A. Surzhykov, S. Fritzsche, and Th. Stöhlker, Photon-photon angular correlations in the radiative recombination of bare high-z ions, *Journal of Physics B: Atomic, Molecular and Optical Physics* **35**, 3713 (2002).
- [30] A. Surzhykov, U. D. Jentschura, T. Stöhlker, and S. Fritzsche, Radiative electron capture into high-Z few-electron ions: Alignment of the excited ionic states, *Phys. Rev. A* **73**, 032716 (2006).
- [31] Th. Stöhlker, F. Bosch, A. Gallus, C. Kozhuharov, G. Menzel, P. H. Mokler, H. T. Prinz, J. Eichler, A. Ichihara, T. Shirai, R. W. Dunford, T. Ludziejewski, P. Rymuza, Z. Stachura, P. Swiat, and A. Warczak, Strong alignment observed for the time-reversed photoionization process studied in relativistic collisions with bare uranium ions, *Phys. Rev. Lett.* **79**, 3270 (1997).
- [32] Th. Stöhlker, Collision spectroscopy of highly charged ions at the esr storage ring, *Phys. Scripta* **1999**, 165 (1999).
- [33] D.R. Bates, Excitation of the 1s-2p transition of atomic hydrogen by proton and alpha particle impact, *Proc. Phys. Soc.* **77**, 59 (1961).
- [34] A.V. Maiorova, A.A. Peshkov, and A. Surzhykov, Structured ion beams produced by radiative recombination of twisted electrons, *Phys. Rev. A* **101**, 062704 (2020).